Supplementary Information

Axial oxygen-bridged FeN_4O/NC produced by ultrafast joule heating for efficient oxygen reduction reaction

Feng Liu,[a,1] Xinyu Guo,[a,1] Yan Zhong,[a] Shaqi Fu,[a] Jingsha Li,[a] Chunmei Zhang,[a] Heng Zhang,[a] Fenghui Ye,[b] Shuai Yuan,[c] Chuangang Hu*[b] and Chunxian Guo*[a]

[a] Institute of Materials Science and Devices, School of Materials Science and Engineering, Suzhou University of Science and Technology, Suzhou 215009, China.

[b] State Key Laboratory of Organic-Inorganic Composites, College of Chemical Engineering, Beijing University of Chemical Technology, Beijing 100029, China.

[c] School of Software and Microelectronics, Peking University, Beijing 102600, China.

[1] These authors contributed equally.

*Corresponding authors

E-mail: cxguo@usts.edu.cn (C. Guo)
chuangang.hu@mail.buct.edu.cn (C. Hu)

Experimental Section

Preparation of NC. 2.23 g zinc nitrate was dissolved in 50 mL methanol as solution A; 2.44 g 2-methimidazole were dissolved in 50 mL methanol, named solution B, solution A was poured into solution B, adjusting the reaction speed to 800 rpm for 24 h. The resulting solution was centrifuged at 12,000 rpm for 2 min, washed twice with methanol, and finally dried in vacuum at 60 °C. The obtained product was denoted as ZIF-8. The precursor ZIF-8 was heat-treated at 950 °C in Ar atmosphere for 2 hours with a heating rate of 5 °C min^{-1} and then naturally cooled to room temperature, respectively. The resulted product were denoted as NC.

Preparation of FeN_4O/NC and FeN_4/NC. 50 mg of NC was dispersed in 100 mL of *N, N*-Dimethylformamide (DMF) by ultrasound for 2 h. Thereafter 0.3 mL of $[Fe(Phen)_3]^{2+}$ ethanol solution (50 mg mL^{-1}, prepared by dissolving ferrous acetate ($Fe(Ac)_2$) and 1,10 phenanthroline (phen) with molar ratio of 1:3 in ethanol) were added drop-wise into the above dispersion with vigorous stirring. The resulting mixture was stirred and allowed to adsorb at room temperature for 12 h. The adsorbed mixture was washed three times with acetone in a centrifuge at 12,000 rpm for 2 min, with the resulting $[Fe(Phen)_3]^{2+}$/NC ovendried at 60 °C to obtain the desired precursor. The precursor $[Fe(Phen)_3]^{2+}$/NC was placed into the graphite tubes and subjected to the periodic carbothermal shock treatment (Input current: 100 A; 3 s-heating and 6 s-cooling is one cycle, total 14 cycles) using the Joule heating equipment (Hefei In-situ Technology Co., Ltd. Anhui, China) in an argon atmosphere. The resulted product were denoted as FeN_4O/NC (i.e. FeN_4O/NC-0.3). Similarly, when 0.1 and 0.5 mL of $[Fe(Phen)_3]^{2+}$ ethanol solution were introduced, FeN_4O/NC-0.1 and FeN_4O/NC-0.5 were prepared. The synthesis of FeN_4/NC involved the introduction of 100 mL of ethanol in place of 100 mL of DMF, the following procedures were identical to the preparation of FeN_4O/NC.

Materials Characterization. Scanning electron microscopy (SEM) images were obtained from Zeiss Gemini 300 scanning electron microscope. Transmission electron microscopy (TEM), high resolution transmission electron microscopy (HRTEM),

high-annular dark-field scanning TEM (HAADF-STEM), and EDS were conducted on a JEOL JEM-2200FS transmission electron microscope. Aberration-corrected High-angle annular dark-field scanning transmission electron microscopy (HAADF-STEM) images were performed with a JEOL JEM-ARM 200F transmission electron microscope with a probe corrector operated at 200 kV. The X-ray absorption fine structure spectra (XAFS) spectra at the Fe K-edge were measured at 1W1B station in Beijing Synchrotron Radiation Facility (BSRF, operated at 2.5 GeV with a maximum current of 250 mA). The spectra of samples were recorded in fluorescence excitation mode using a Lytle detector. The spectra of Fe foil and Fe_2O_3 were used as references, and recorded in a transmission mode using ionization chamber. The crystal phases of the samples were characterized by a Bruker D2 Phaser X-ray diffractometer with a Cu Kα radiation source (30 kV, 10 mA). Raman spectra were recorded using a Horibal LabRAM HR Evolution Raman spectrometer operating with a laser wavelength of 532 nm. The nitrogen adsorption and desorption isotherms were studied by using a Micrometrics ASAP 2460 Specific surface and porosity analyzer. The specific surface area and pore size distribution were calculated from the nitrogen adsorption-desorption isotherms. X-ray photoelectron spectroscopy (XPS) measurements were carried out on a Kratos AXIS SUPRA X-ray photoelectron spectrometer with an Al Kα radiation (15 kV, 10 mA).

Electrochemical Measurements. The oxygen reduction reaction (ORR) activities of catalysts were measured by a CHI Electrochemical workstation (model 760c) with a standard three-electrode system at room temperature. The catalyst-coated glassy carbon rotating disk electrode (RDE, 5 mm in diameter) or rotating ring-disk electrode (RRDE, disk outer diameter, ring inner diameter and ring outer diameter are 5.61 mm, 6.25 mm, and 7.92 mm, respectively) was used as the working electrode, an Ag/AgCl electrode in saturated KCl solution was used as the reference electrode, and graphite rod was used as counter electrode. All of the potentials reported in this paper were calibrated to the reversible hydrogen electrode. To prepare a homogeneous catalyst ink, 3 mg of catalyst was dispersed in a solution of 147 μL of deionized water,

147 μL of isopropanol and 6 μL of a Nafion solution (5 wt%, Alfa Aesar D521) under sonication for 2 h. Then 7.5 μL of catalyst ink were loaded onto the glassy carbon and dried in air. A Pt/C (20 wt% of Pt, Johnson Mattery HiSPEC) catalyst with a loading of 40 μg $_{Pt}$ cm^{-2} was used as a reference. Linear scan voltammetry (LSV) tests were carried out in O_2-saturated 0.1 M KOH solution with a scan rate of 5 mV s^{-1}. Four-electron selectivity during the ORR was determined by measuring LSV curves on RDE at various rotating speeds (625, 900, 1225, 1600, and 2025 rpm). The corresponding electron transfer number was determined from the slope of the linear line according to the following Koutechy-Levich (K-L) equation:

$$\frac{1}{J}=\frac{1}{J_{\mathrm{L}}}+\frac{1}{J_{\mathrm{K}}}=\frac{1}{B\omega^{1/2}}+\frac{1}{J_{\mathrm{K}}}$$

$$B=0.62nF(D_0)^{2/3}(\nu)^{-1/6}C_0 \quad (1)$$

where J, J_{L}, J_{K} are the measured current density, diffusion-limiting current density, and kinetic current density, respectively. ω is the angular velocity of the disk (ω = $2\pi N$, N is the rotation speed), n is the electron transfer number, F is the Faraday constant (F = 96,485 C mol^{-1}), D_0 is the diffusion coefficient of oxygen (D_0 = 1.9 × 10^{-5} cm^2 s^{-1}, 0.1 M KOH), C_0 is the bulk concentration of oxygen (C_0 = 1.2 × 10^{-6} mol cm^{-3}, 0.1 M KOH), ν is the kinetic viscosity of the electrolyte (ν = 0.01 cm^2 s^{-1}). The electron transfer number (n) and the yield of H_2O_2 were calculated from the RRDE measurement based on the disk current (I_{d}) and ring current (I_{r}) via the following equations:

$$n=4\times\frac{I_{\mathrm{d}}}{I_{\mathrm{d}}+I_{\mathrm{r}}/N} \quad (2)$$

$$\mathrm{H_2O_2}\%=200\times\frac{I_{\mathrm{r}}}{(I_{\mathrm{r}}+NI_{\mathrm{d}})} \quad (3)$$

Where N = 0.37 is the current collection efficiency of Pt ring.

Zn-air battery test. The home-made zinc-air battery device has been employed for the battery performance measurements. The electrolyte used for the electrochemical liquid zinc-air battery was 6 M KOH and 0.2 M $Zn(Ac)_2$ aqueous solution. Typically,

5 mg catalysts mixed with 20 μL Nafion solution (5 wt%, Alfa Aesar D521) were dispersed in 490 μL of deionized water and 490 μL of isopropanol solution by sonicating for 2 h to form a homogeneous ink. The obtained catalyst ink was then brushed onto a piece of carbon paper with an effective area of 1 cm^2 until the loading amount reaching 1 mg cm^{-2}, which was serving as the cathode for Zn-air battery. A polished zinc plate (0.1 mm thickness) was used as the anode. As a reference material, 20 wt% Pt/C catalysts were prepared as the same procedure and the Pt/C loading on the carbon was 1.0 mg cm^{-2}. All the Zn-air batteries were tested under ambient atmosphere. Discharge polarization and power density curves were measured on CHI 760E electrochemical workstation (CHI Instruments, Inc., Shanghai). The glavanostatic discharge test were performed on a LAND CT2001A testing system.

Computational details. The density functional theory (DFT) calculations were carried out using the DMol3[1] module implemented in Material Studio. The GGA method as implemented with Perdew, Burke, and Ernzerhof (PBE-GGA)[2, 3] was used to describe the exchange-correlation functional component of the Hamiltonian. The k point grids were set as 2 × 2 × 1 for the Brillouin zone and a large vacuum slab of 15 Å is inserted in z direction for surface isolation to prevent interaction between two neighboring surfaces. The convergence threshold for the iteration in self-consistent-field (SCF) is set to be 10^{-5} eV. A smearing of 0.005 Ha (1 Ha = 27.21 eV) to the orbital occupation was applied. The geometry convergence tolerance for energy change, max force and max displacement were 1×10^{-5} Ha, 0.002 Ha/Å, 0.005 Å, respectively.

The ORR proceeds for four-electron pathway in alkaline electrolyte are shown as follows:[4]

$$* + O_2 + H_2O + e^- \rightarrow OOH^* + OH^- \quad (4)$$

$$OOH^* + e^- \rightarrow O^* + OH^- \quad (5)$$

$$O^* + H_2O + e^- \rightarrow OH^* + OH^- \quad (6)$$

$$OH^* + e^- \rightarrow * + OH^- \quad (7)$$

Where * refers to an active site on the catalysts surface.

The reaction Gibbs free energy changes (ΔG) were calculated by the following equation:

$$\Delta G = \Delta E + \Delta ZPE - T\Delta S + \Delta G_{pH} + \Delta G_U \quad (8)$$

Where ΔE is obtained directly from DFT calculation results, ΔZPE is the correction of zero point vibration energy (ZPE), T is the room temperature of 298.15K, and ΔS is the correction for entropy. $\Delta G_{pH} = -K_B T \ln[H^+] = pH \times K_B T \ln 10$,[5] is the change of free energy owing to the effect of pH value of the electrolyte. $\Delta G_U = -neU$, is the effect of the electrons transfer in the electrode and the electrode potential contribution to ΔG.

Supplementary Figures

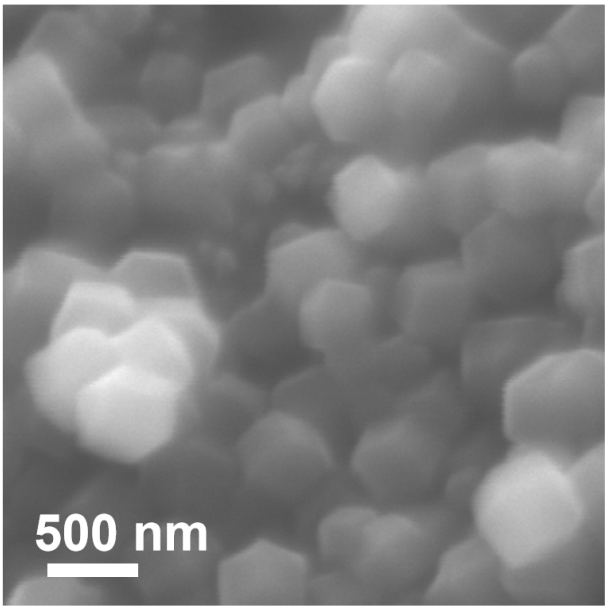

Fig. S1. SEM image of NC.

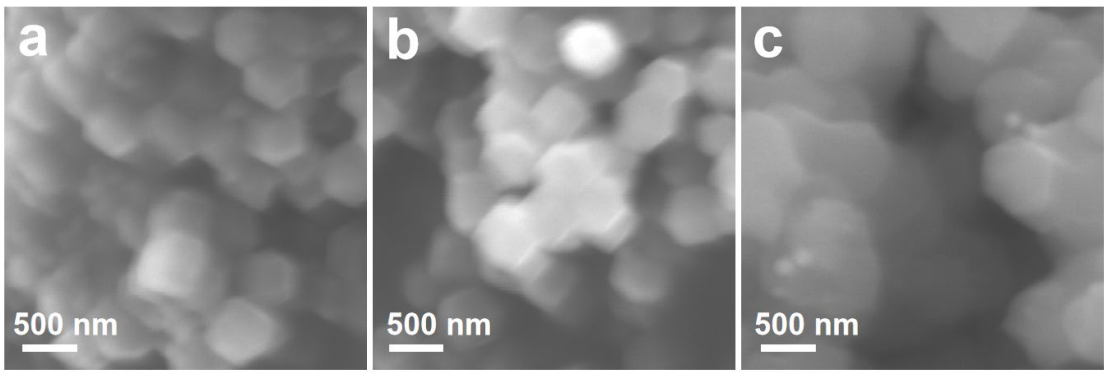

Fig. S2. SEM images of of FeN_4O/NC-0.1, FeN_4O/NC-0.3, and FeN_4O/NC-0.5 prepared with different $[Fe(Phen)_3]^{2+}$ ethanol solution addition.

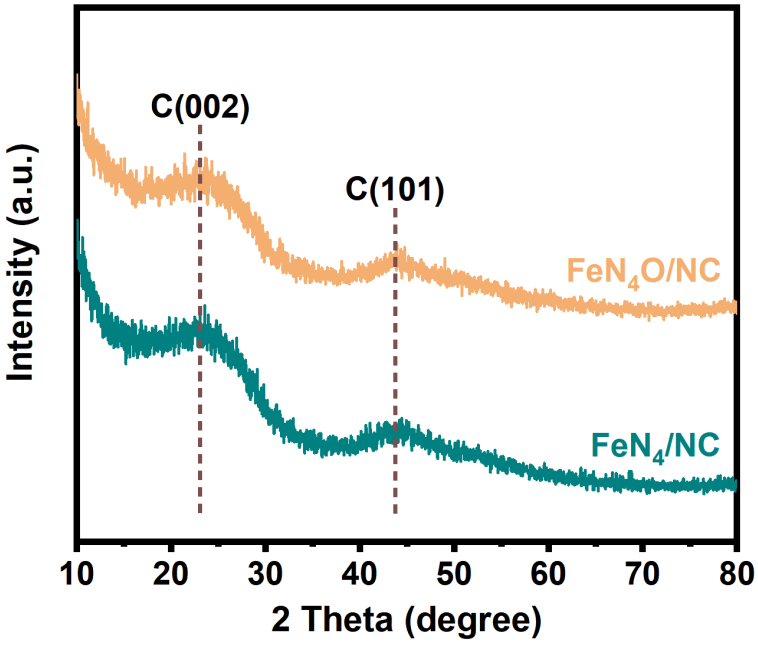

Fig. S3. XRD patterns of FeN_4O/NC and FeN_4/NC.

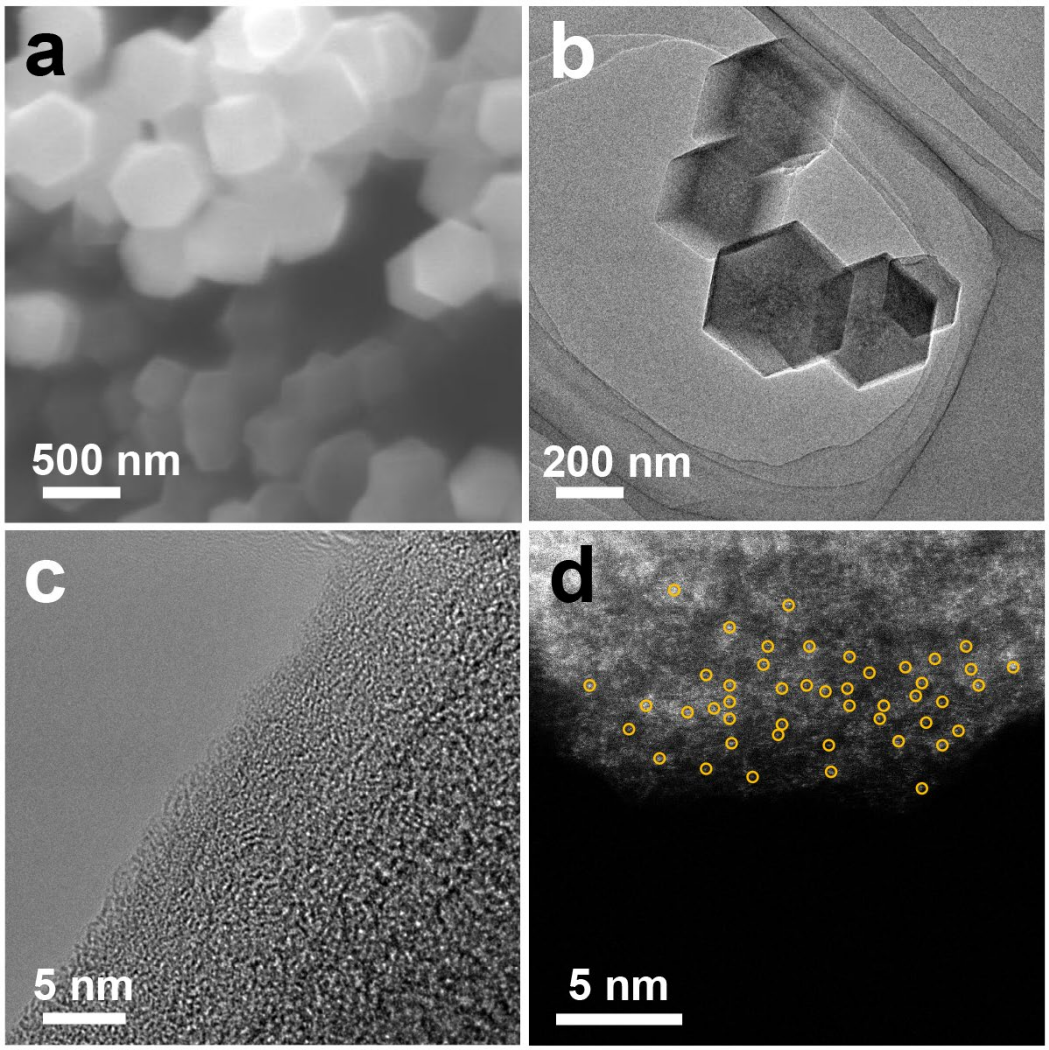

Fig. S4 (a) SEM and (b) TEM images of FeN_4/NC. (c) HRTEM and (d) AC HAADF-STEM images of FeN_4/NC.

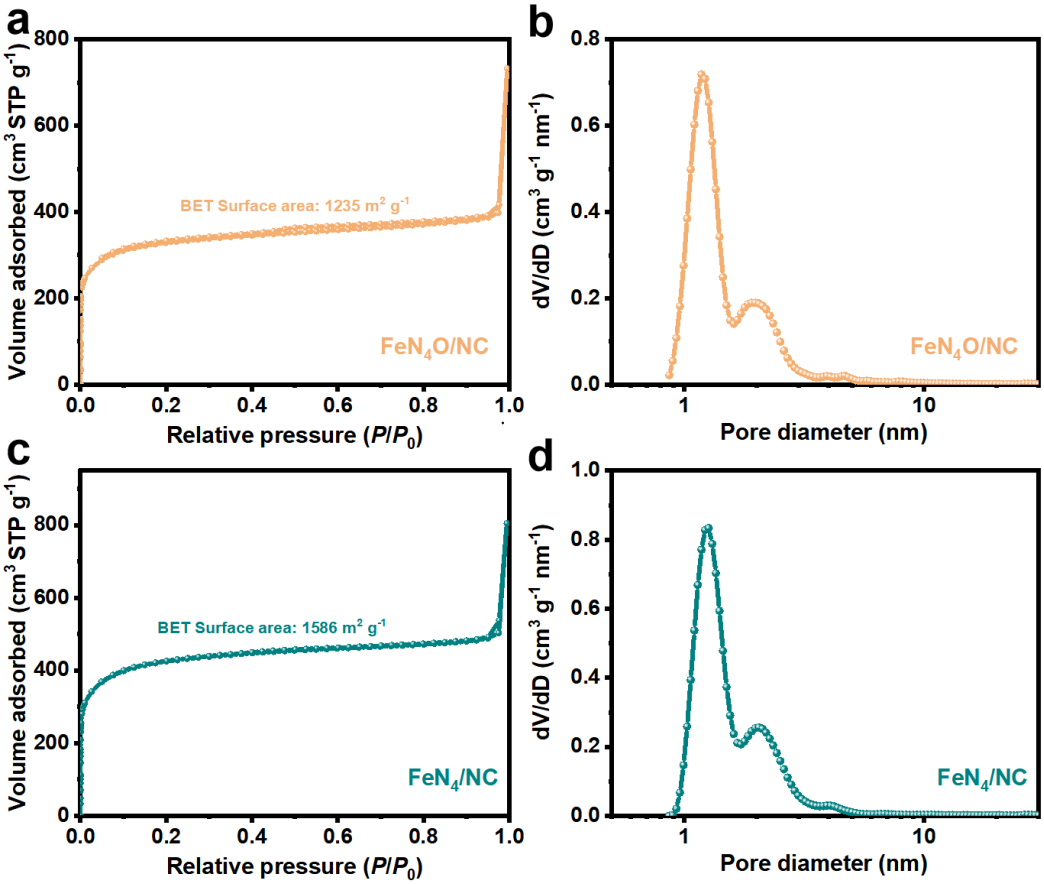

Fig. S5. N_2 adsorption-desorption isotherms of (a) FeN_4O/NC and (c) FeN_4/NC. Corresponding pore size distribution curves of (b) FeN_4O/NC and (d) FeN_4/NC.

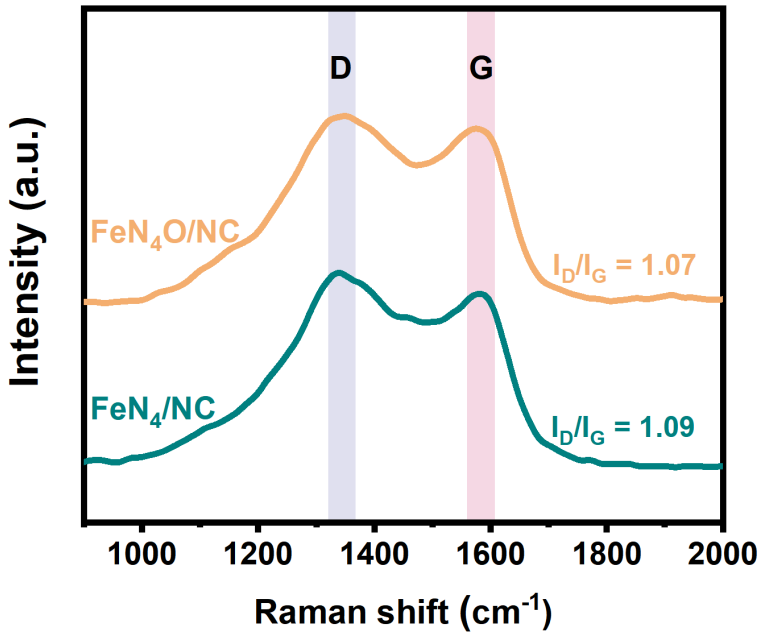

Fig. S6. Raman spectra of FeN_4O/NC and FeN_4/NC.

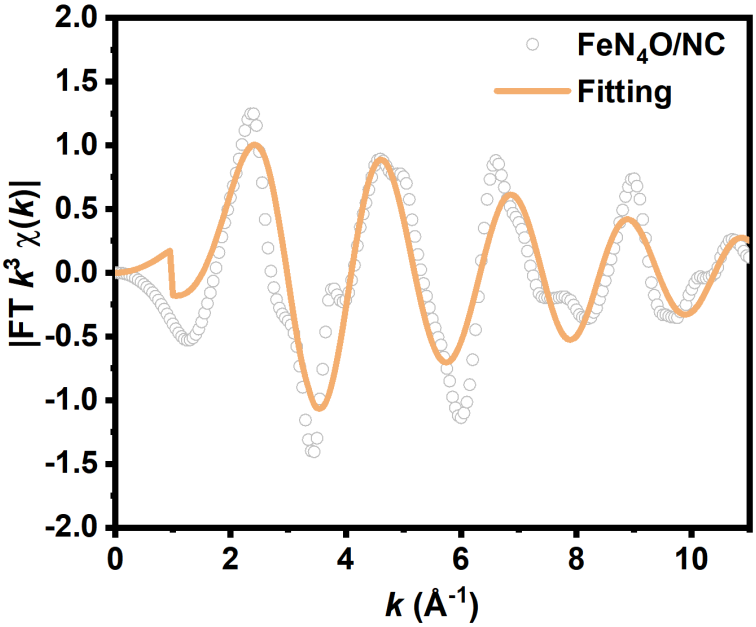

Fig. S7. The corresponding FT-EXAFS k-space fitting curve of FeN_4O/NC.

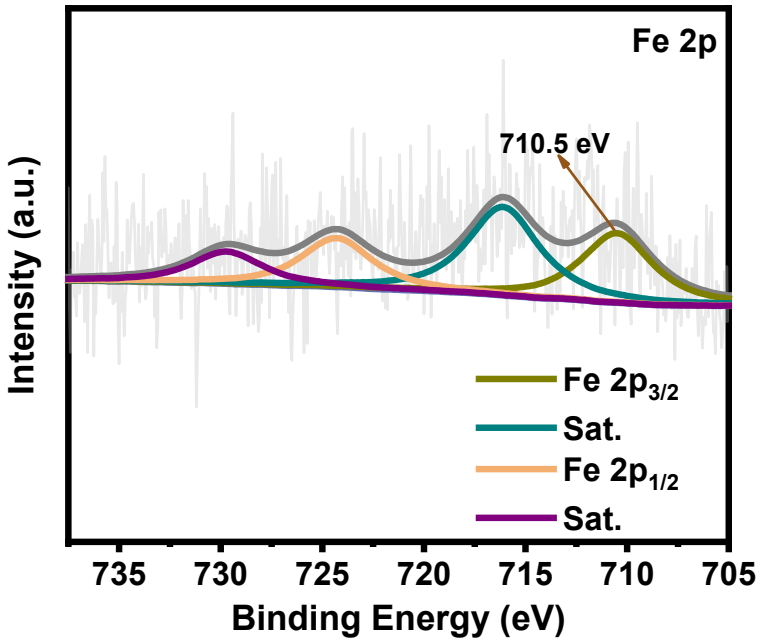

Fig. S8. High-resolution Fe 2p XPS spectrum of FeN_4/NC.

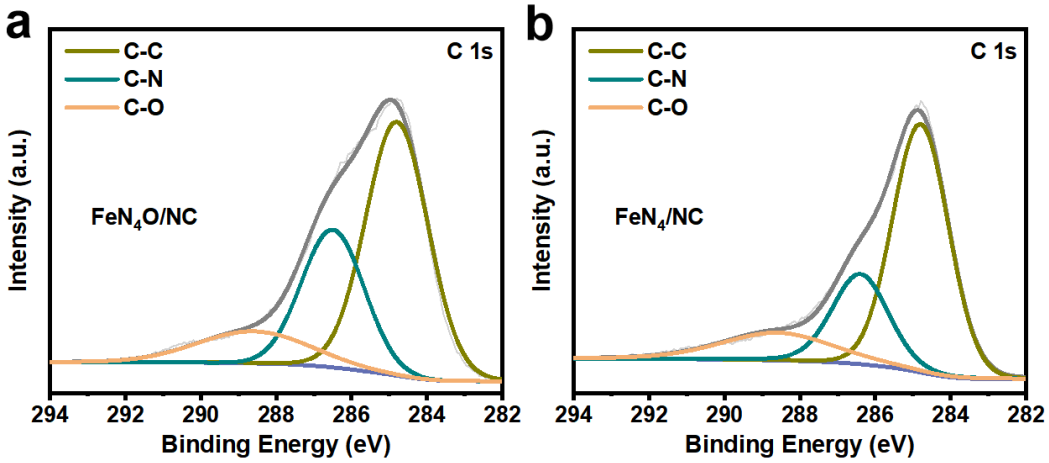

Fig. S9. High-resolution C 1s XPS spectra of (a) FeN_4O/NC and (b) FeN_4/NC.

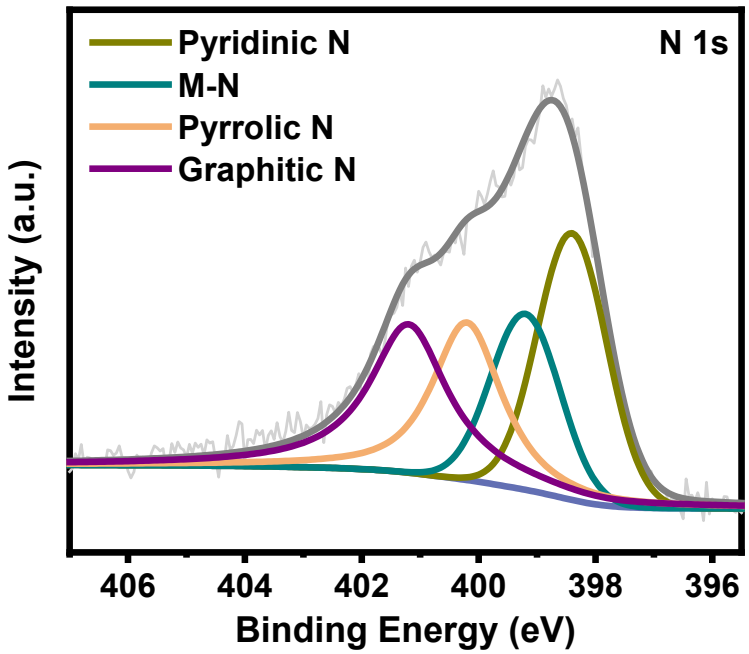

Fig. S10. High-resolution N 1s XPS spectrum of FeN_4/NC.

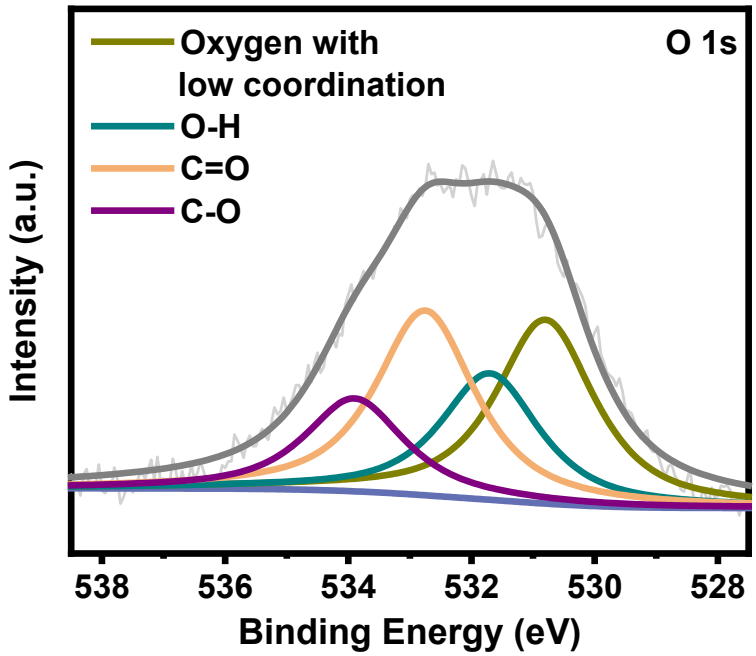

Fig. S11. High-resolution O 1s XPS spectrum of FeN_4/NC.

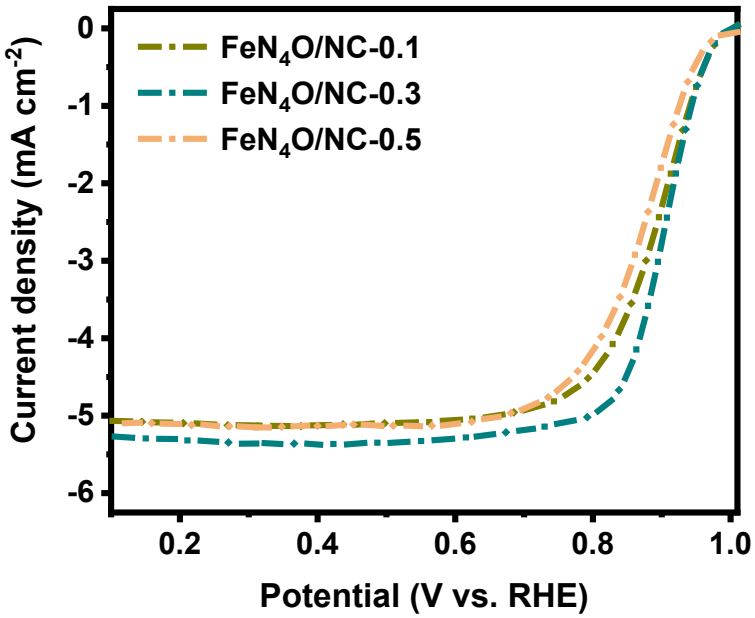

Fig. S12. ORR polarization curves of FeN_4O/NC-0.1, FeN_4O/NC-0.3, and FeN_4O/NC-0.5 in O_2-saturated 0.1 M KOH solution with a scan rate of 5 mV S^{-1} and a rotation rate of 1600 rpm.

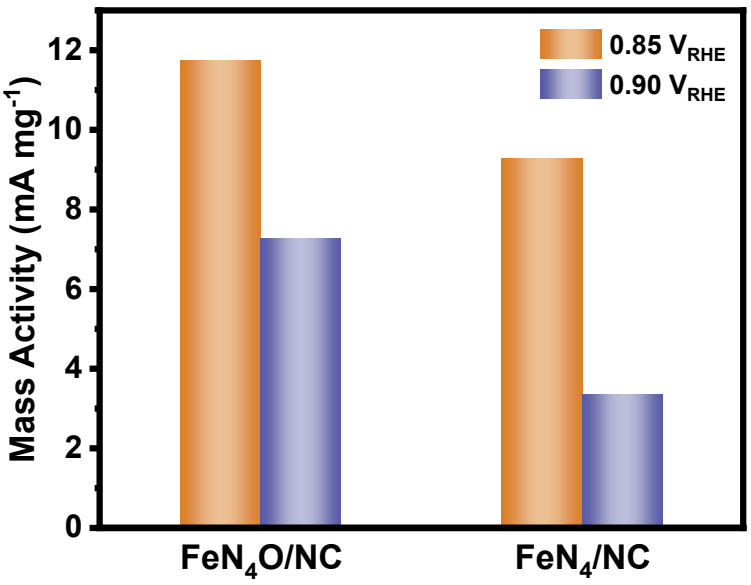

Fig. S13. A comparison of the mass activities of FeN_4O/NC and FeN_4/NC catalysts at 0.85 V and 0.90 V versus RHE.

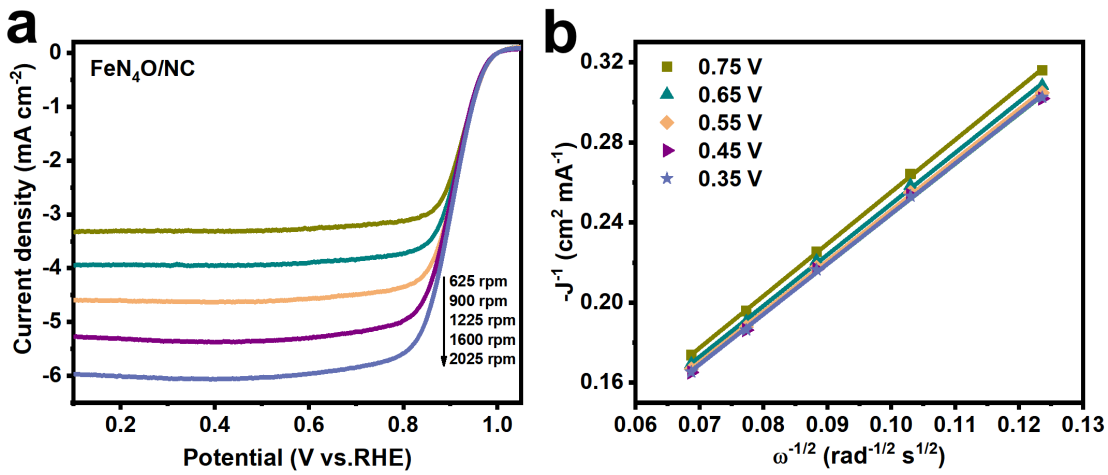

Fig. S14. (a) ORR polarization curves of FeN_4O/NC at various rotation rates. (b) Corresponding K-L plots.

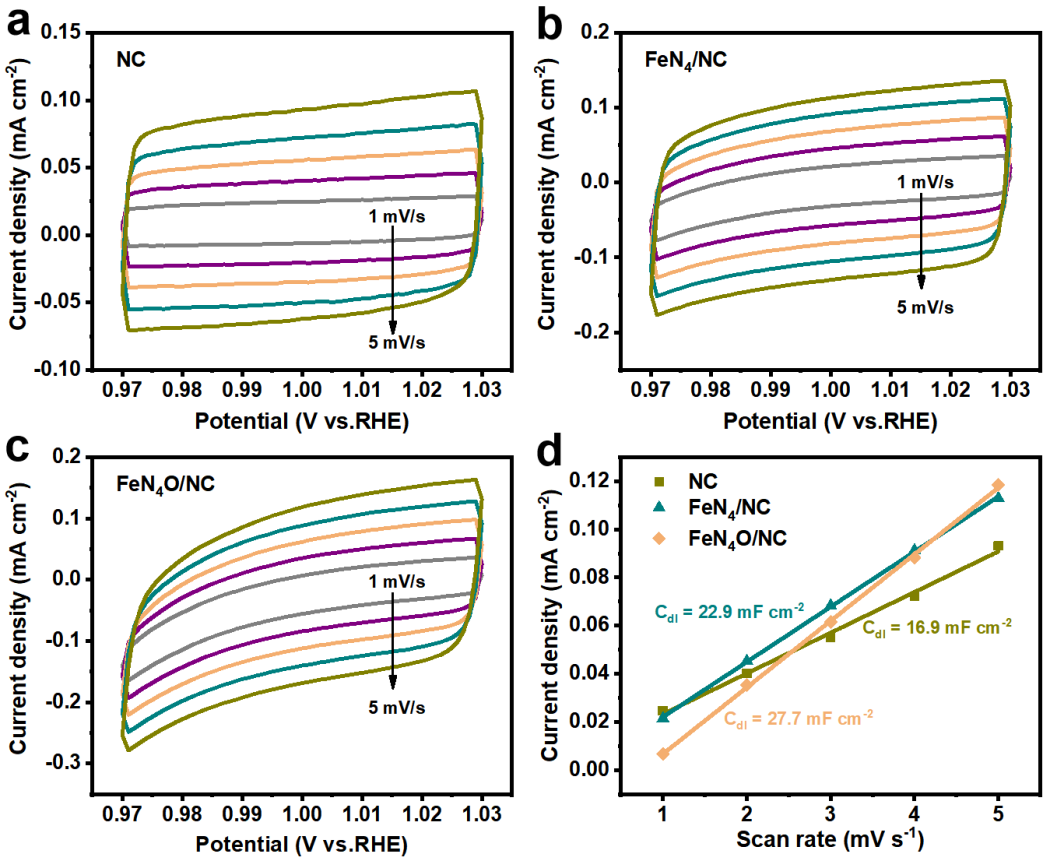

Fig. S15. Cyclic voltammograms curves of (a) NC, (b) FeN_4/NC and (c) FeN_4O/NC at different scan rates (1, 2, 3, 4 and 5 mV/s) in the region of 0.97-1.03 V vs. RHE for ORR. (d) Electrochemical double-layer capacitance (C_{dl}) of NC, FeN_4/NC and FeN_4O/NC.

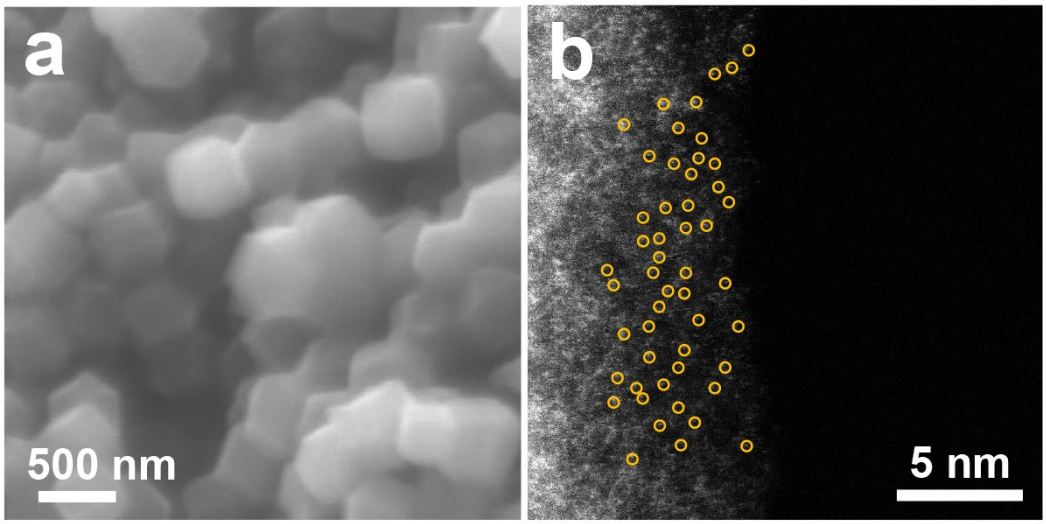

Fig. S16. (a) SEM and (b) AC HAADF-STEM images of the used FeN_4O/NC after durability test.

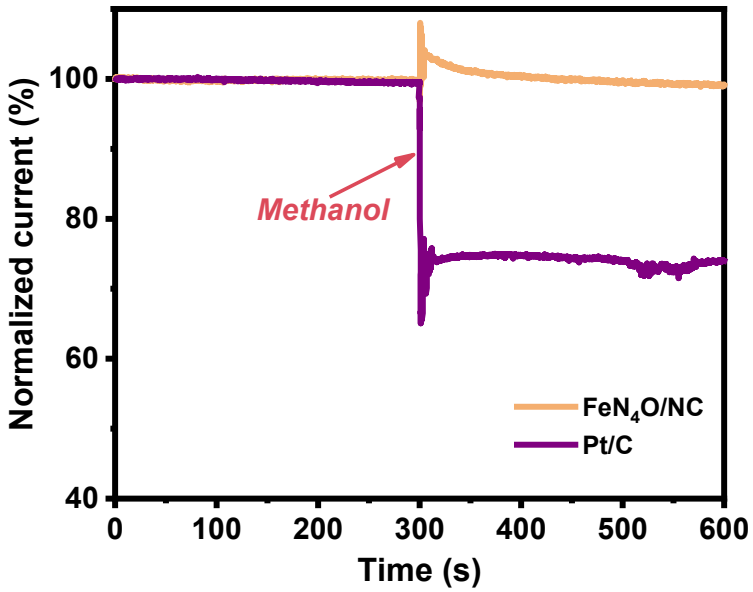

Fig. S17. Methanol resistance test of FeN_4O/NC and Pt/C.

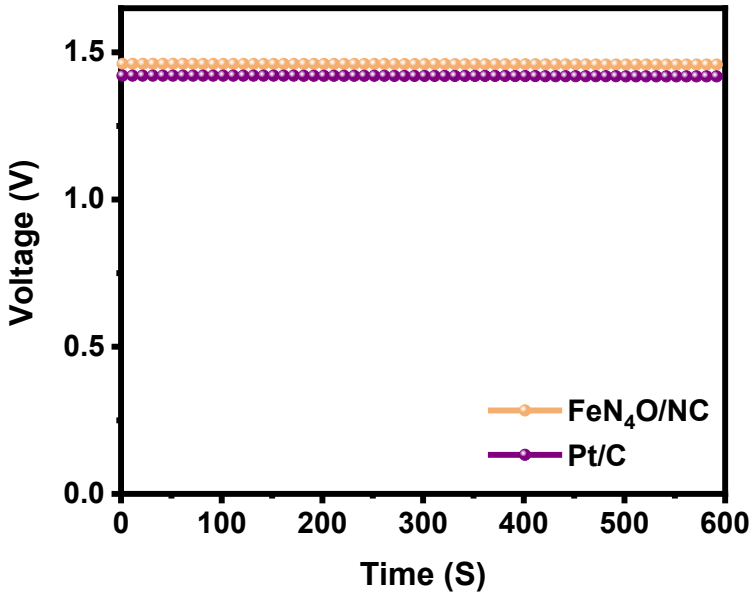

Fig. S18. Open-circuit potentials (OCV) of Zn-air batteries with FeN_4O/NC and Pt/C as the air cathode catalysts, respectively.

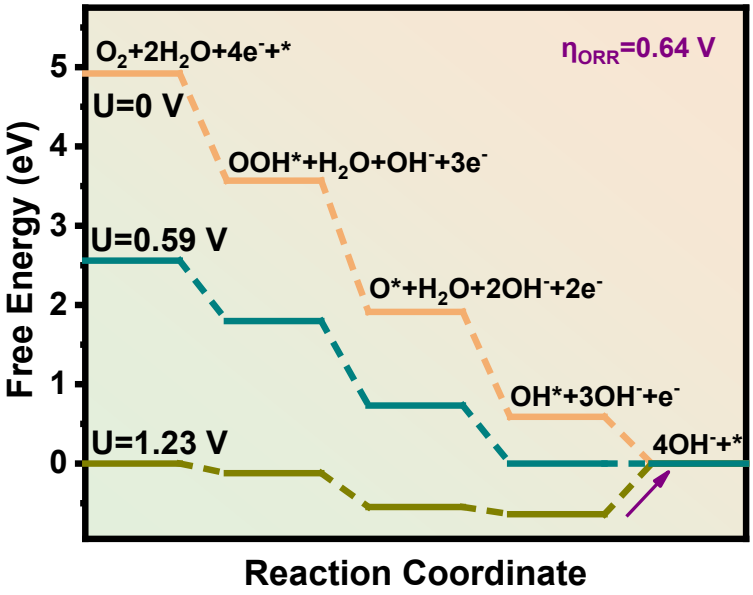

Fig. S19. ORR free-energy diagrams of FeN_4/NC model.

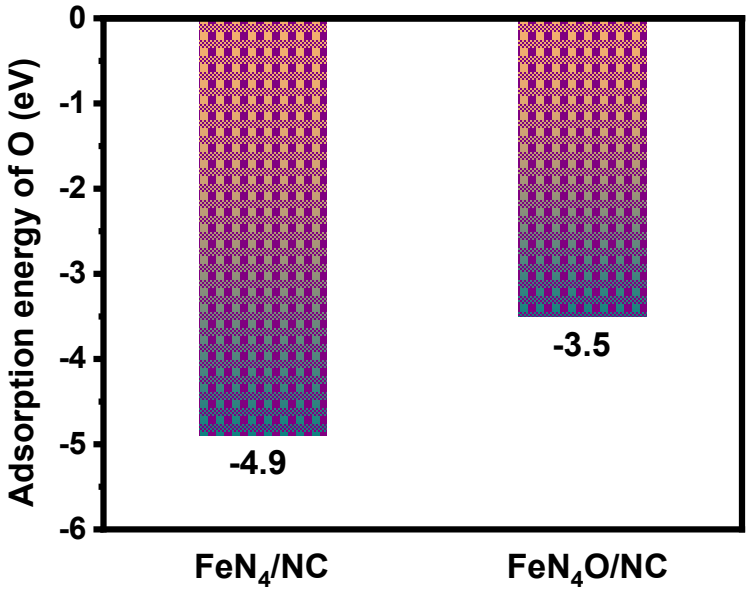

Fig. S20. Adsorption energy of O on the central Fe atom in FeN_4/NC and FeN_4O/NC sites.

Supplementary Tables

Table S1. The values of specific surface area, total pore volume and micropore volume of FeN_4O/NC and FeN_4/NC catalysts.

Sample	S_{BET} (m^2 g^{-1})	Total pore volume (cm^3 g^{-1})	Micropore volume (cm^3 g^{-1})
FeN_4O/NC	1235	0.56	0.34
FeN_4/NC	1586	0.53	0.38

Table S2. XPS elemental quantification of FeN_4O/NC and FeN_4/NC catalysts.

Sample	C (at%)	N (at%)	O (at%)	Fe (at%)
FeN_4O/NC	82.32	7.91	9.15	0.62
FeN_4/NC	83.51	7.57	8.24	0.68

Table S3. The iron contents of FeN_4O/NC-0.1, FeN_4O/NC-0.3, and FeN_4O/NC-0.5 prepared with different $[Fe(Phen)_3]^{2+}$ ethanol solution addition determined by ICP-OES.

Sample	Fe (weight percentage, %)
FeN_4O/NC-0.1	0.52
FeN_4O/NC-0.3	0.71
FeN_4O/NC-0.5	0.82

Table S4. ORR activity comparison of FeN_4O/NC with previously reported highly active non-precious metal catalysts.

Catalyst	Loading (mg cm^{-2})	Electrolyte	$E_{1/2}$ (V vs. RHE)	Reference
FeN_4O/NC	**0.38**	**0.1 M KOH**	**0.903**	**This work**
HCNT@Co-NC	0.4	0.1 M KOH	0.85	*Chem. Commun.* **2024**, 60, 1476-1479.
Fe_2/NC	0.51	0.1 M KOH	0.90	*Angew. Chem. Int. Ed.* **2024**, e202413179.
Fe_2-pPc	0.255	0.1 M KOH	0.92	*J. Am. Chem. Soc.* **2024**, 146, 24842-24854.
FeCo/DA@NC	0.306	0.1 M KOH	0.84	*Small* **2024**, 20, 2305390.
CoCOP-COOH@KB	0.25	0.1 M KOH	0.86	*Nat. Commun.* **2024**, 15, 6077.
Fe-Co-NC	0.408	0.1 M KOH	0.88	*Adv. Funct. Mater.* **2024**, 2408257.
FeSn-C_2N	0.4	0.1 M KOH	0.914	*J. Am. Chem. Soc.* **2024**, 146, 21357-21366.
Cl-FeN_4	0.5	0.1 M KOH	0.92	*Adv. Funct. Mater.* **2024**, 2409794.
FeN_4Cl-SAzyme	-	0.1 M KOH	0.885	*Chem. Commun.* **2023**,59, 3550-3553.
Zn-N_4-O	0.4	0.1 M KOH	0.884	*Adv. Sci.* **2023**, 10, 2302152.
Mn SAs/Fe_3C NPs@NPC	0.5	0.1 M KOH	0.88	*Nano Res.* **2022**, 15, 7976-7985.
Ru-SAS/SNC	0.4	0.1 M KOH	0.861	*J. Am. Chem. Soc.* **2022**, 144, 2197-2207.
V-N-C SAC	0.4	0.1 M KOH	0.858	*Chem. Eng. J.* **2022**, 444, 136363.
r-Fe-NC	0.6	0.1 M KOH	0.90	*Sci. Bull.* **2022**, 67, 1264-1273.
d-SA-FeNC	-	0.1 M KOH	0.90	*ACS Catal.* **2022**, 12, 5397-5406
Fe SA-NSC-900	0.1	0.1 M KOH	0.86	*ACS Energy Lett.* **2021**, 6, 379-386.
Co_1-N_3PS/HC	0.51	0.1 M KOH	0.92	*Angew. Chem. Int. Ed.* **2021**, 60, 3212-3221.
Fe/OES	0.4	0.1 M KOH	0.85	*Angew. Chem. Int. Ed.* **2020**, 132, 7454-7459.
E-FeNC	0.5	0.1 M KOH	0.875	*Appl. Catal. B: Environ.* **2020**, 265, 118593

References

[1] B. Delley, *J. Chem. Phys.* **2000**, *113*, 7756.

[2] J. P. Perdew, K. Burke and M. Ernzerhof, *Phys. Rev. Lett.* **1996**, *77*, 3865.

[3] J. P. Perdew, K. Burke and M. Ernzerhof, *Phys. Rev. Lett*. **1997**, *78*, 1396.

[4] Z. Yang, Y. Wang, M. Zhu, Z. Li, W. Chen, W. Wei, T. Yuan, Y. Qu, Q. Xu, C. Zhao, X. Wang, P. Li, Y. Li, Y. Wu, Y. Li, *ACS Catal.* **2019**, *9*, 2158.

[5] J. K. Norskov, J. Rossmeisl, A. Logadottir, L. Lindqvist, J. R. Kitchin, T. Bligaard, H. Jonsson, *J. Phys. Chem. B* **2004**, *108*, 17886.